Advances and Applications in Mechanical Engineering and Technology
Volume 3, Number 1/2, 2011, Pages 59-81

STUDY OF CONCENTRATED VERTICAL LOAD AT THE APEX OF A WEDGE BY THE EXPERIMENTAL METHODS OF CAUSTICS AND PHOTOELASTICITY

G. A. PAPADOPOULOS

Department of Mechanics
National Technical University of Athens
5, Heroes of Polytechnion Av.
GR-157 73, Zografou
Athens
Greece
e-mail: gpad@central.ntua.gr

Abstract

The experimental method of caustics was used for the evaluation of the stress-singularities created by concentrated load applied at the apex of a wedge or on the horizontal straight boundary of a half-plane. It was proved that the shape and size of the caustic depend on the stress singularity at the point of application of the load. The parametric equations of caustics created by such a singularity were studied in relation with the loading mode of the wedge. Also, the stress singularity created by a concentrated load applied at the apex of the wedge or on the horizontal straight boundary of a half-plane was studied by isochromatic fringes of photoelasticity. Thus, by measuring the dimensions of the caustic, one can evaluate the state of stress at the singularity. The relations for the calculation of the load, the components of stress and the concentration factor based on the geometrical characteristic of caustics and on isochromatic fringes were given.

Keywords and phrases: contact problem, caustics, photoelasticity, isochromatic, isopachic, concentration factor.

Received May 26, 2011

1. Introduction

The optical method of caustics is suitable for the experimental study of singularities in stress fields created either by geometric discontinuities or by loading. For many crack problems, the stress intensity factors at the crack-tip were calculated by caustics [6, 7, 13]. Contact problems and wedge problems have many practical and important applications [16]. For the solution of such problems, besides mechanical analysis, the experimental method of caustics can also be applied. Caustics have been applied to the study of the singular stress fields developed near concentrated or uniformly distributing loads, which are applied along straight boundaries [2, 14, 15]. Also, the method of caustics was applied to study the load sharing in roller-bearings [8, 9] and in multiple gear tooth contact [11, 12]. Also, three-dimensional wedge problems, bimaterial wedges in antiplane shear deformation, and rubber wedges in large strain analysis were studied [1, 5, 10].

The aim of the present work is to give the parametric equations of the caustics in wedges, which were made of isotropic materials, for the case of a concentrated vertical load at the apex of the wedge. Also, the relations of calculation of the concentrated force at the apex of wedge, the components of stress at any point and the concentration factor of the stresses based on the diameter, the opening displacement of the caustic and isochromatic fringes were given. Also, an experimental application in bearing model was given.

2. Concentrated Vertical Load at the Apex of the Wedge

Concentrated vertical load P (compressive load) is applied on the direction of axis of the wedge (Figure 1). The thickness of the wedge is taken as unity. The conditions along the faces, $\theta = \pm\varphi$, of the wedge are satisfied by the stress components, which are derived from the stress function [16].

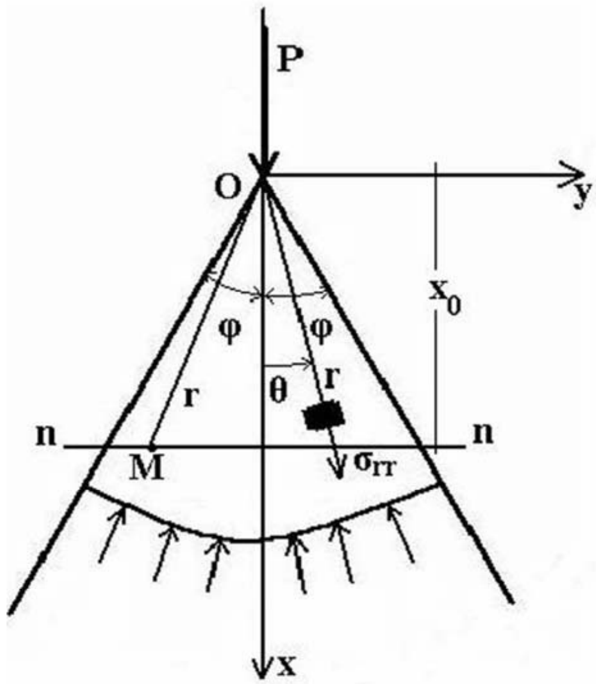

Figure 1. Geometry of a symmetrical wedge of angle 2φ.

$$\Phi = -\frac{P}{2\left(\varphi + \frac{1}{2}\sin 2\varphi\right)} r\theta \sin\theta, \tag{1}$$

where P is the concentrated vertical load (load per wedge thickness unity), φ is the angle of wedge, and r, θ are the polar coordinates.

The stress components are derived from Equation (1) as

$$\sigma_{rr} = \frac{1}{r}\frac{\partial \Phi}{\partial r} + \frac{1}{r^2}\frac{\partial^2 \Phi}{\partial \theta^2} = -\frac{P}{\varphi + \frac{1}{2}\sin 2\varphi}\frac{\cos\theta}{r}, \tag{2}$$

$$\sigma_{\theta\theta} = \frac{\partial^2 \Phi}{\partial r^2} = 0, \tag{3}$$

$$\tau_{r\theta} = -\frac{\partial}{\partial r}\left(\frac{1}{r}\frac{\partial \Phi}{\partial \theta}\right) = 0. \tag{4}$$

By taking $\varphi = \pi / 2$, the solution for a semi-infinite plate was given, which has been studied by the method of caustics and photoelasticity method [8, 9].

3. Experimental Method of Caustics

The divergent light rays, which are reflected from the front face of the specimen, form wave fronts

$$S(x, y, z) = \text{const.}. \tag{5}$$

If $s(x, y)$ expresses the optical path of the light ray between two planes parallel to the middle plane of the loaded plate and lying at the faces of the plate, then the relation

$$S(x, y, z) = z - s(x, y) = \text{const.} \tag{6}$$

is valid and

$$\text{grad} S(x, y, z) = \mathbf{k} - \frac{\partial s}{\partial x} \mathbf{i} - \frac{\partial s}{\partial y} \mathbf{j}, \tag{7}$$

where $\mathbf{i}$, $\mathbf{j}$, and $\mathbf{k}$ are the unit vectors of the (Ox, y, z) Cartesian coordinates system. For optically isotropic materials and for the first light ray reflected from the front (f) face of the specimen, the deviation of the light rays at a distance z_0 from the middle plane of the specimen, is expressed by the vector $\mathbf{w}$ on the plane $z = z_0$, and according to the theory of Econal [3], is given as

$$\mathbf{w}_f = -\frac{z_0 d c_f}{\lambda_m} \text{grad}(\sigma_1 + \sigma_2), \tag{8}$$

where d is the thickness of the specimen, c_f is the stress-optical constant, which is given by the relation

$$c_f = -\frac{\nu}{E}, \tag{9}$$

where ν is the Poisson's ratio, E is the elastic modulus, and λ_m is the magnification ratio, which is given by the relation

$$\lambda_m = \frac{z_0 + z_i}{z_i}, \tag{10}$$

where z_0 is the distance between reference-plane and specimen and z_i is the distance between specimen and the light beam focus. The sum of the stresses $\sigma_1 + \sigma_2$ is given by

$$\sigma_1 + \sigma_2 = \sigma_{rr} + \sigma_{\theta\theta} = -\frac{P}{\varphi + \frac{1}{2}\sin 2\varphi}\frac{\cos\theta}{r}. \tag{11}$$

Then, Equation (8) becomes

$$\mathbf{w}_f = C_f \mathrm{grad}_{(x,y)}\left(\frac{1}{r}\cos\theta\right) = C_f \frac{1}{r^2}[\cos 2\theta\mathbf{i} + \sin 2\theta\mathbf{j}], \tag{12}$$

where

$$C_f = -\frac{z_0 d c_f P}{\lambda_m(\varphi + \frac{1}{2}\sin 2\varphi)}. \tag{13}$$

The parametric equations of the caustic are

$$\mathbf{W}_f = \mathbf{r} + \mathbf{w}_f,$$

or

$$X_f = r\cos\theta + C_f r^{-2}\cos 2\theta,$$

$$Y_f = r\sin\theta + C_f r^{-2}\sin 2\theta. \tag{14}$$

The initial curve of the caustic, which is placed at the singular region of concentrated load, is determined by setting the functional determinant Jacobian J equal to zero according to

$$J = \frac{\partial(X_t, Y_t)}{\partial(r, \theta)} = 0.$$

Then, the initial curve is

$$r_0 = r = (2C_f)^{1/3}. \tag{15}$$

By substituting Equation (15) into Equations (14), it is found that the parametric equations of the caustic for divergent light beam reflected from the front face of the plate (caustic (f)), which is compressed, are

$$X_f = \lambda_m (2C_f)^{\frac{1}{3}} \left[\cos\theta + \frac{1}{2}\cos 2\theta \right], \tag{16}$$

$$Y_f = \lambda_m (2C_f)^{\frac{1}{3}} \left[\sin\theta + \frac{1}{2}\sin 2\theta \right]. \tag{17}$$

The parametric equations of caustics formed from divergent light rays, which are reflected from the rear face of the plate (caustic (r)), are

$$X_r = \lambda_m (2C_r)^{\frac{1}{3}} \left[\cos\theta - \frac{1}{2}\cos 2\theta \right],$$

$$Y_r = \lambda_m (2C_r)^{\frac{1}{3}} \left[\sin\theta - \frac{1}{2}\sin 2\theta \right],$$

with

$$C_r = -\frac{2z_0 d c_r P}{\lambda_m \left(\phi + \frac{1}{2}\sin 2\phi\right)},$$

where c_r is the stress-optical constant.

For values of θ between $-\varphi$ and $+\varphi$, the initial curve and the respective caustic are obtained around the point of the concentrated load P. Figure 2 illustrates the forms of the respective caustics (f) and (r) and the initial curve for wedge of angle $\varphi = \pi / 4$.

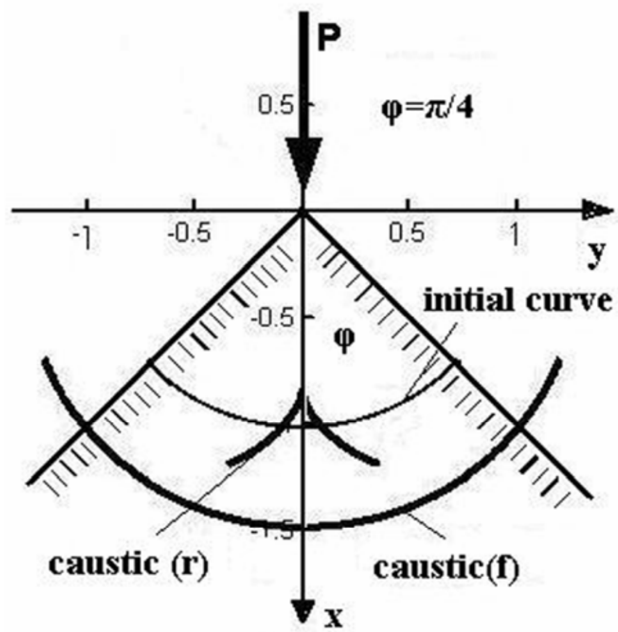

Figure 2. The respective caustics (f) and (r) and the initial curve plotted at the apex of wedge angle $\varphi = \pi / 4$.

Figure 3 illustrates the forms of the respective caustics (f) and (r) and the initial curve for wedge of angle $\varphi = \pi / 2$. In this figure, the maximum diameter $D_{\max}$ and the opening displacement L of the caustic (f) are appeared.

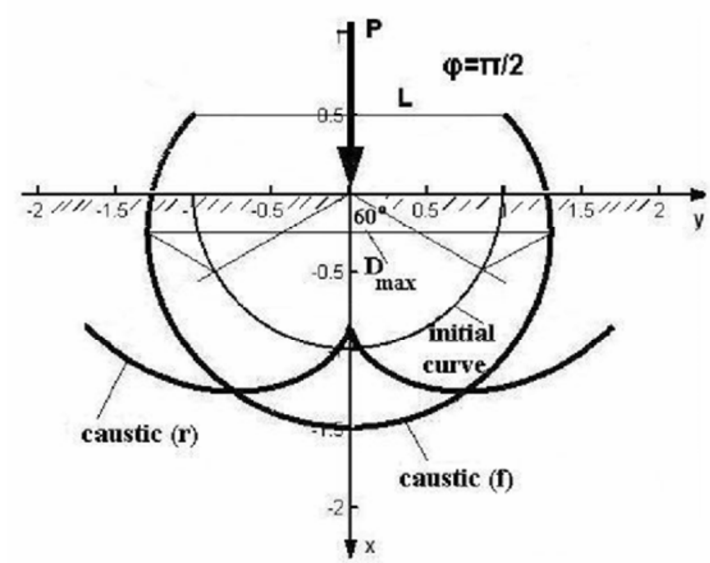

Figure 3. The respective caustics (f) and (r) and the initial curve plotted at the apex of wedge angle $\varphi = \pi / 2$.

Figure 4 illustrates the forms of the respective caustics (f) and (r) and the initial curve for wedge of angle $\varphi = 3\pi / 4$.

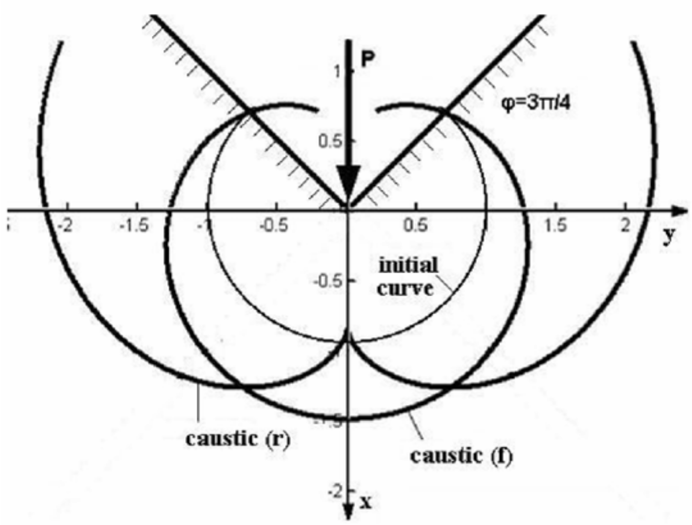

Figure 4. The respective caustics (f) and (r) and the initial curve plotted at the apex of wedge angle $\varphi = 3\pi / 4$.

The maximum diameter of the caustic along the Oy-axis (Figure 3), can be derived from the condition

$$\frac{\partial Y_f}{\partial \theta} = 0, \tag{18}$$

which gives

$$\theta^{\max} = 60°. \tag{19}$$

Relation (16), for $\theta = \theta^{\max} = 60^{\circ}$, gives

$$D_{\max} = 2Y_f^{\max} = 2.598\lambda_m r_0 = 3.273\lambda_m C_f^{1/3}. \tag{20}$$

By substituting Equation (13) into Equation (20) results

$$P = 0.0285 \frac{\varphi + \frac{1}{2}\sin 2\varphi}{z_0 d\lambda_m^2 c_f} D_{\max}^3. \tag{21}$$

From Equation (21), the load P can be experimentally estimated from the diameter of the caustic that is formed at the point of applied the force. For angles of wedge $\varphi < 60°$, the diameter of the caustic has not presented maximum. In these cases, the load P can be calculated from the opening displacement L of the caustic (Figure 3). The opening displacement L is given

$$L = 2Y_f\big|_{\theta=\varphi} = 2\lambda_m r_0(\sin\varphi + \frac{1}{2}\sin 2\varphi) = 2.52\lambda_m C_f^{1/3}(\sin\varphi + \frac{1}{2}\sin 2\varphi). \tag{22}$$

By substituting Equation (13) into Equation (22) gives

$$P = \frac{L^3}{16 z_0 d\lambda_m^2 c_f} \frac{\varphi + \frac{1}{2}\sin 2\varphi}{\left[\sin\varphi + \frac{1}{2}\sin 2\varphi\right]^3}. \tag{23}$$

The stress function, the stress, and the load P for various angles of the wedge are given in Table 1.

Table 1. The stress function, the stress, and the load for various wedge angles

ϕ	**Stress function** Φ	**Stress** σ_r	**Load** P	**Load** P
$\pi/12$	$\frac{\Phi}{\mathrm{Pr}\,\theta\sin\theta} = -0.977$	$\frac{\sigma_r}{P\frac{\cos\theta}{r}} = -1.954$	$\frac{P}{\frac{L^3}{z_0 d\lambda_m^2 c_f}} = 0.243$	
$\pi/6$	– 0.523	– 1.046	0.073	
$\pi/4$	– 0.389	– 0.778	0.046	
$\pi/3$	– 0.338	– 0.676	0.042	$\frac{P}{\frac{D_{\max}^3}{z_0 d\lambda_m^2 c_f}} = 0.042$
$\pi/2$	– 0.318	– 0.636	0.098	0.045
$2\pi/3$	– 0.301	– 0.602	1.278	0.047
$3\pi/4$	– 0.270	– 0.540	4.219	0.053

The relation between opening displacement L and the maximum diameter $D_{\max}$ of the caustic is obtaining by comparing the Equations (21) and (23)

$$\frac{L}{D_{\max}} = 0.77\left(\sin\varphi + \frac{1}{2}\sin 2\varphi\right). \tag{24}$$

The relation (24) is valid for wedge angles $\varphi \geq \pi/3$. The ratio $L/D_{\max}$ for various wedge angles is given in Table 2.

Table 2. The ratio of the opening displacement and the diameter of the caustic for various wedge angles

Wedge angle φ	**Ratio** $L/D_{\max}$
$\pi/3$	1.00
$\pi/2$	0.77
$2\pi/3$	0.33
$3\pi/4$	0.16
π	0

Figure 5 illustrates the experimental reflected caustics (f) and (r), for divergent light beam, in specimen of wedge angle $\varphi = \pi / 2$ made of Plexiglas of thickness $d = 3 \times 10^{-3}$m. Also, Figure 6 illustrates the experimental transmitted caustic, for convergent light beam, in specimen of wedge angle $\varphi = 3\pi / 4$ made of Plexiglas of thickness $d = 3 \times 10^{-3}$m.

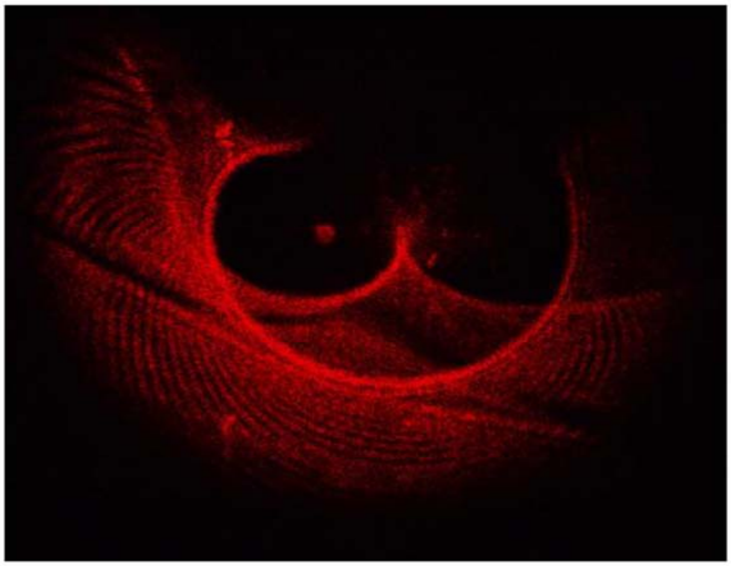

Figure 5. Experimental reflected caustics (f) and (r) for divergent light beam in specimen of wedge angle $\varphi = \pi / 2$.

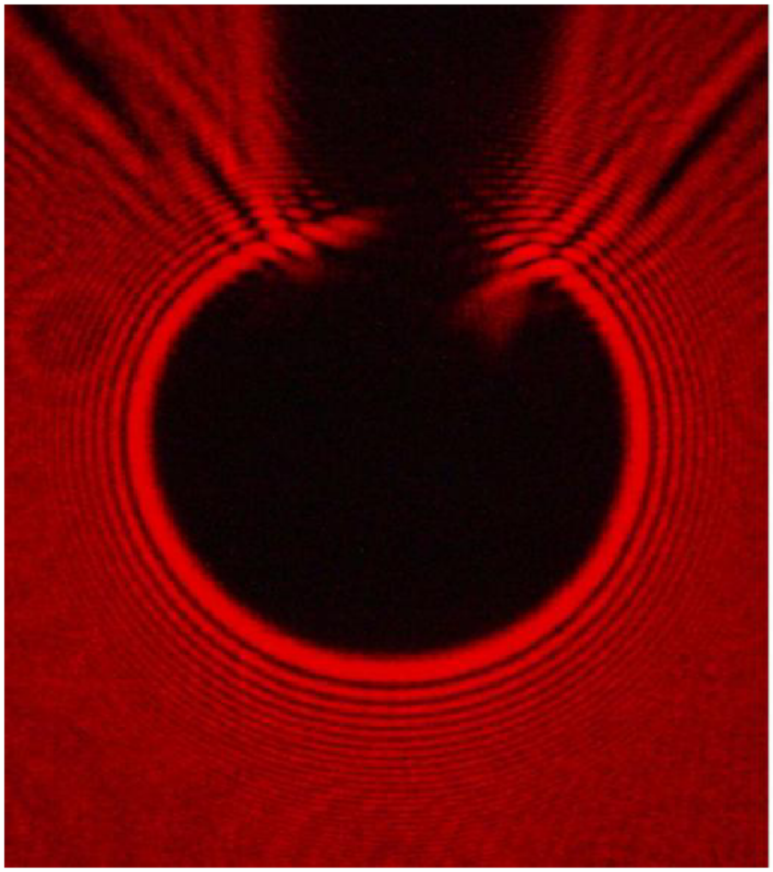

Figure 6. Experimental transmitted caustics for convergent light beam in specimen of wedge angle $\varphi = 3\pi / 4$.

4. Calculation of the Stresses σ_{ij}

On the horizontal plane nn at a distance x_0 from the apex of the wedge, the stress components at any point M (Figure 1) are calculated from the polar stress component σ_{rr}

$$\sigma_{xx} = \sigma_{rr} \cos^2 \theta = -\frac{P}{\varphi + \frac{1}{2} \sin 2\varphi} \frac{\cos^3 \theta}{r} = -\frac{P}{\varphi + \frac{1}{2} \sin 2\varphi} \frac{\cos^4 \theta}{x_0}, \tag{25}$$

$$\sigma_{yy} = \sigma_{rr} \sin^2\theta = -\frac{P}{\varphi + \frac{1}{2}\sin 2\varphi} \frac{\cos\theta \sin^2\theta}{r} = -\frac{P}{\varphi + \frac{1}{2}\sin 2\varphi} \frac{\cos^2\theta \sin^2\theta}{x_0}, \tag{26}$$

$$\tau_{xy} = \sigma_{rr} \sin\theta\cos\theta = -\frac{P}{\varphi + \frac{1}{2}\sin 2\varphi} \frac{\sin\theta \cos^2\theta}{r} = -\frac{P}{\varphi + \frac{1}{2}\sin 2\varphi} \frac{\sin\theta\cos^3\theta}{x_0}, \tag{27}$$

with

$$r = x_0 / \cos\theta. \tag{28}$$

By substituting Equations (21) and (23) into Equations (25)-(27), the components of stress are obtained from the diameter and opening displacement of the caustic

$$\begin{aligned}\sigma_{xx} &= -0.0285 \frac{D_{\max}^3}{z_0 d\lambda_m^2 c_f} \frac{\cos^4\theta}{x_0}\bigg|_{\varphi \geq 60^\circ} \\ &= -\frac{L^3}{16 z_0 d\lambda_m^2 c_f \left[\sin\varphi + \frac{1}{2}\sin 2\varphi\right]^3} \frac{\cos^4\theta}{x_0}\bigg|_{\text{for any } \varphi},\end{aligned} \tag{29}$$

$$\begin{aligned}\sigma_{yy} &= -0.0285 \frac{D_{\max}^3}{z_0 d\lambda_m^2 c_f} \frac{\cos^2\theta \sin^2\theta}{x_0}\bigg|_{\varphi \geq 60^\circ} \\ &= -\frac{L^3}{16 z_0 d\lambda_m^2 c_f \left[\sin\varphi + \frac{1}{2}\sin 2\varphi\right]^3} \frac{\cos^2\theta \sin^2\theta}{x_0}\bigg|_{\text{for any } \varphi},\end{aligned} \tag{30}$$

$$\begin{aligned}\tau_{xy} &= -0.0285 \frac{D_{\max}^3}{z_0 d\lambda_m^2 c_f} \frac{\cos^3\theta \sin\theta}{x_0}\bigg|_{\varphi \geq 60^\circ} \\ &= -\frac{L^3}{16 z_0 d\lambda_m^2 c_f \left[\sin\varphi + \frac{1}{2}\sin 2\varphi\right]^3} \frac{\cos^3\theta \sin\theta}{x_0}\bigg|_{\text{for any } \varphi}.\end{aligned} \tag{31}$$

For a horizontal plane *nn* close to the apex of the wedge at a distance equals to the radius of the initial curve of the caustic

$$x_0 = r_0 = \frac{D_{\max}}{2.598\lambda_m}\Big|_{\varphi \geq 60^\circ} = \frac{L}{2\left(\sin\varphi + \frac{1}{2}\sin 2\varphi\right)\lambda_m}\Big|_{\text{for any } \varphi}, \tag{32}$$

the components of stress, Equations (29)-(31), are

$$\sigma_{xx} = -0.074\,\frac{D^2_{\max}}{z_0 d\lambda_m c_f}\cos^4\theta\Big|_{\varphi \geq 60^\circ}$$

$$= -\frac{L^2}{8z_0 d\lambda_m c_f\left[\sin\varphi + \frac{1}{2}\sin 2\varphi\right]^2}\cos^4\theta\Big|_{\text{for any } \varphi}, \tag{33}$$

$$\sigma_{yy} = -0.074\,\frac{D^2_{\max}}{z_0 d\lambda_m c_f}\cos^2\theta\sin^2\theta\Big|_{\varphi \geq 60^\circ}$$

$$= -\frac{L^2}{8z_0 d\lambda_m c_f\left[\sin\varphi + \frac{1}{2}\sin 2\varphi\right]^2}\cos^2\theta\sin^2\theta\Big|_{\text{for any } \varphi}, \tag{34}$$

$$\tau_{xy} = -0.074\,\frac{D^2_{\max}}{z_0 d\lambda_m c_f}\cos^3\theta\sin\theta\Big|_{\varphi \geq 60^\circ}$$

$$= -\frac{L^2}{8z_0 d\lambda_m c_f\left[\sin\varphi + \frac{1}{2}\sin 2\varphi\right]^2}\cos^3\theta\sin\theta\Big|_{\text{for any } \varphi}, \tag{35}$$

for values of θ between $-\varphi$ and $+\varphi$.

Figure 7 illustrates the distribution of the non-dimensional components of stress (Equations (33)-(35)),

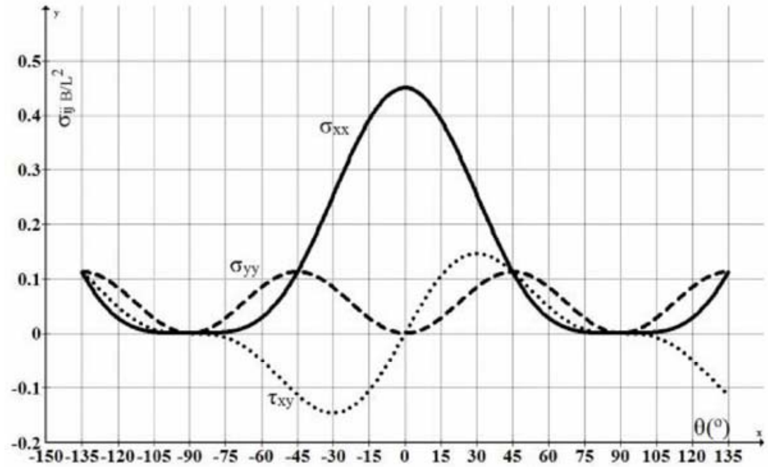

Figure 7. The stress components variation versus θ for wedge angles up to $\varphi = 3\pi / 4$.

$$\sigma_{ij} \frac{B}{L^2} = f(\theta) \quad \text{with} \quad B = -8 z_0 d \lambda_m c_f \left[\sin\varphi + \frac{1}{2} \sin 2\varphi \right]^2,$$

on the horizontal plane at distance r_0 (singular region of concentrated load) from the wedge apex (Figure 1), for wedges of angle up to $\varphi = 3\pi / 4$.

5. Concentration Factor K_w

From Equations (25)-(27), the function of components of stress can be written

$$\begin{aligned} \sigma_{xx} &= -K_w \frac{\cos^3\theta}{r}, \\ \sigma_{yy} &= -K_w \frac{\cos\theta \sin^2\theta}{r}, \\ \tau_{xy} &= -K_w \frac{\cos^2\theta \sin\theta}{r}, \end{aligned} \tag{36}$$

where K_w is the concentration factor of the stresses for the wedge of angle 2φ. This concentration factor is given by the relation

$$K_w^{th} = \frac{P}{\varphi + \frac{1}{2}\sin 2\varphi}. \tag{37}$$

The variation of the concentration factor for angles φ between 0 and π is illustrated in Figure 8. From Figure 8, it is observed that the concentrated factor is varied between the value 0.318 (for wedge of angle $\varphi = \pi$) and $+\infty$ (for wedge of angle zero degree).

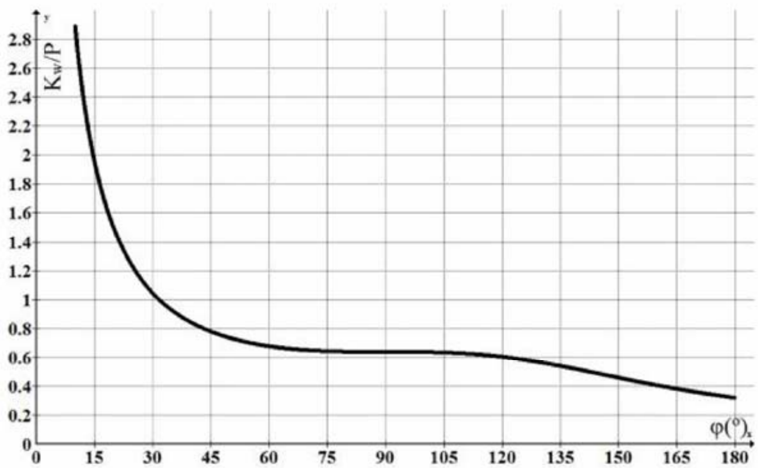

Figure 8. Variation of concentrated factor for wedge angles between 0 and π.

The concentration factor K_w can be experimentally calculated from the caustics by the following relation:

$$K_w^{ex} = 0.0285 \frac{D_{\max}^3}{z_0 d\lambda_m^2 c_f}\Big|_{\varphi \geq 60^\circ} = \frac{L^3}{16 z_0 d\lambda_m^2 c_f \left[\sin\varphi + \frac{1}{2}\sin 2\varphi\right]^3}\Big|_{\text{for any } \varphi}. \tag{38}$$

From relation (37), the theoretical concentration factor, K_w^{th}, while from relation (38), the experimental concentration factor, K_w^{ex}, can be calculated. The concentration factor is depended on the load, the angle of the wedge and the constants of the material. From the ratio $K_w^{ex} / K_w^{th} = f$, a correction factor f for the theoretical concentration factor K_w^{th} can be experimentally calculated, which is depended on the wedge dimensions and the material constants.

6. Photoelastic Method

The concentration factor can be calculated by the photoelastic method at points far away of the wedge apex. According to photoelastic method [4], the difference of principal stresses is obtained from isochromatic fringes

$$\sigma_1 - \sigma_2 = N \frac{f_c}{d} = \sqrt{(\sigma_{xx} - \sigma_{yy})^2 + 4\tau_{xy}^2}, \tag{39}$$

where N is the fringes order and f_c is the stress-optical constant of the material.

By substituting the Equation (36) into Equation (39), we obtain

$$r = \frac{Pd}{f_c} \frac{1}{\varphi + \frac{1}{2}\sin 2\varphi} \frac{|\cos\theta|}{N} = K_w^{ex} \frac{d}{f_c} \frac{|\cos\theta|}{N}, \tag{40}$$

and the concentration factor

$$K_w^{ex} = N \frac{f_c}{d} \frac{r}{|\cos\theta|}, \tag{41}$$

where r and θ are the polar coordinates.

7. Results and Discussion

Figure 9 illustrates the isochromatic fringes in specimen of wedge angle $\varphi = \pi / 4$. Figure 10 illustrates the isochromatic fringes in specimen of wedge angle $\varphi = \pi / 2$.

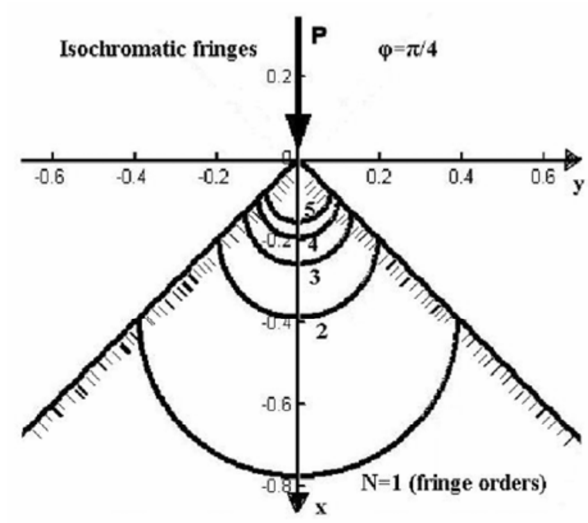

Figure 9. The isochromatic fringes plotted in specimen of wedge angle $\varphi = \pi / 4$.

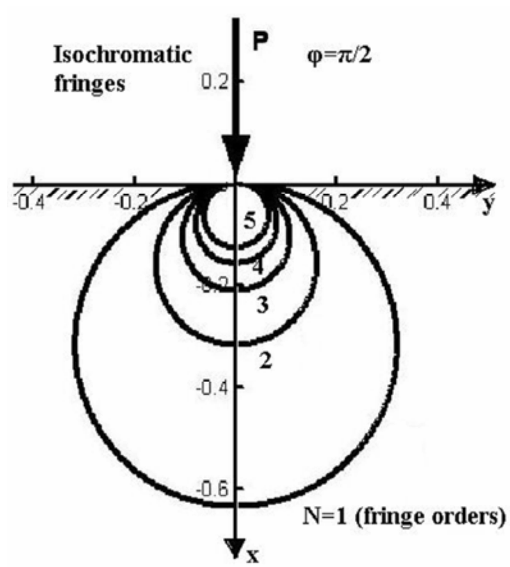

Figure 10. The isochromatic fringes plotted in specimen of wedge angle $\varphi = \pi / 2$.

Figure 11 illustrates the isochromatic fringes in specimen of wedge angle $\varphi = 3\pi / 4$.

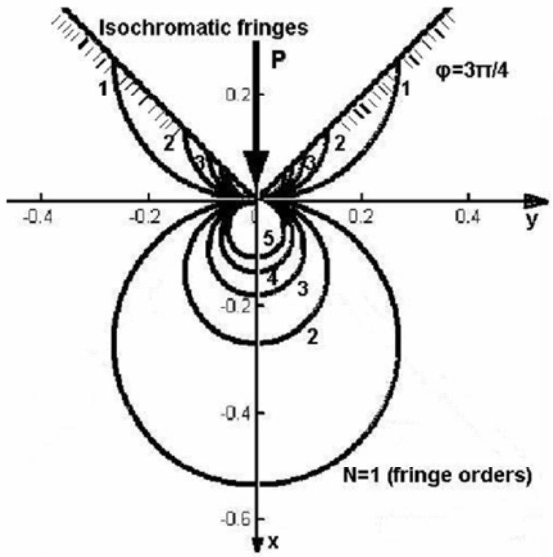

Figure 11. The isochromatic fringes plotted in specimen of wedge angle $\varphi = 3\pi / 4$.

Figure 12 illustrates the experimental isochromatic fringes in specimen of wedge angle $\varphi = 3\pi / 4$ made of epoxy resin of thickness $d = 5 \times 10^{-3}$m. It is appeared that the fringes density at the point of concentrated vertical load (singular point) is high and so, it is difficult to calculate the concentration factor at the singular point (apex of the wedge). The concentration factor can be calculated far away from the singular point (point of concentrated load). The photoelastic method is an experimental method of field and it is not applied exactly at the singular point, i.e., at the crack-tip. The stress intensity factor at the crack-tip or another singular point, is experimentally calculated with accuracy by the caustic, while far from the singular point it can be calculated by the isochromatic fringes.

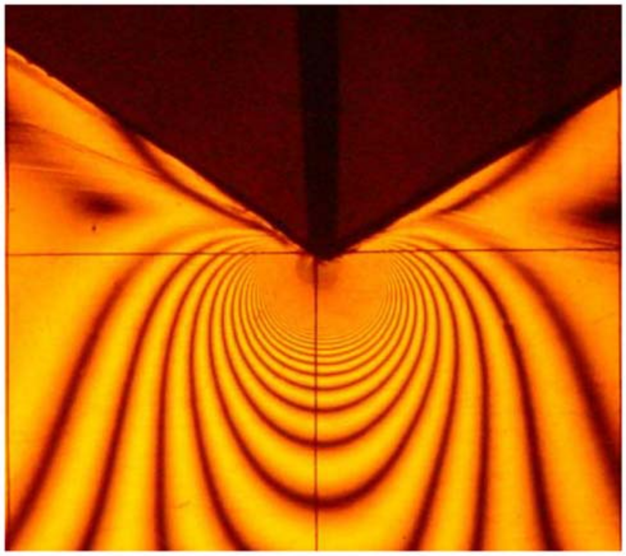

Figure 12. Experimental isochromatic fringes in specimen of wedge angle $\varphi = 3\pi / 4$.

The caustics at the singular point can be plotted by the parametric equations (relations (16) and (17)). The plots were illustrated in Figures 2-4. These plots are corresponded to reflected and transmitted caustics, respectively. The respective experimental caustics are illustrated in Figures 5 and 6. From these experimental caustics, the load and the concentration factor can be calculated. The experimental caustics were formed at the singular point (apex of the wedge). At this point, the isochromatic fringes (Figure 12) can not counted and so the concentration factor can not calculated. Figures 9-11 illustrate the isochromatic fringes plots for five fringe-order, while the Figure 12 illustrates the experimental isochromatic fringes for a highest load. In this figure, the high density of the isochromatic fringes is appeared at the apex of the wedge.

The analysis of the stresses close to apex of the wedge is presented in Figure 7 for various wedge angles. The theoretical variation of the non-dimensional concentration factor is presented in Figure 8 for various wedge angles. The load and the concentration factor can experimentally calculated by the caustic characteristics, maximum diameter or opening displacement (Table 1). The relation between maximum diameter and the opening displacement was presented in Table 2.

An application of the concentration factor experimentally calculation for a bearing model was given. Figure 13 illustrates the transmitted caustics at the contact points between rings and rollers of a bearing for a concentration load P = 44.06KN and for two loaded rollers. The contact points were taken as wedge of angle $\varphi = 90^{\circ}$. The load for each roller, which were symmetrically placed, was about P = 22.03KN. The theoretical and the experimental concentration factors at the contact points A, B, and C were calculated from the maximum diameters of the transmitted caustics by the Equations (37) and (38), with $z_0 = 3.44$m, $d = 0.0093$m, $\lambda_m = 5.3704$, and $c_t = 1.21 \times 10^{-7} \mathrm{m}^2/\mathrm{KN}$.

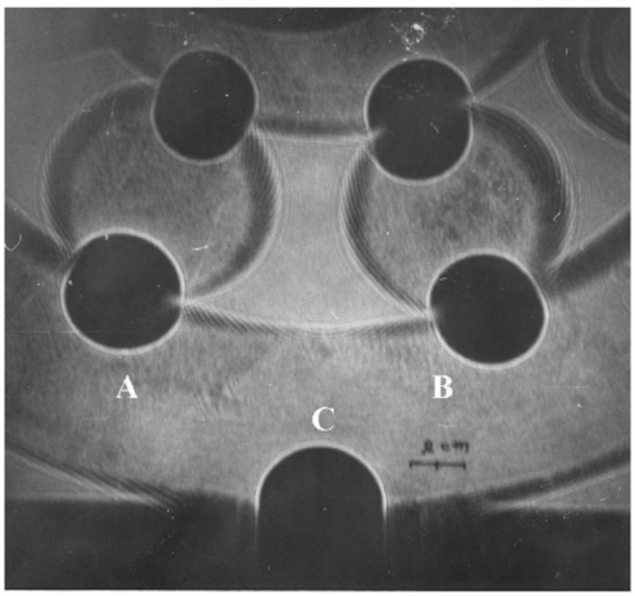

Figure 13. Caustics at the contact points A, B, and C of bearing rollers for an applied load of 44.06 KN.

The calculated concentration factors and the correction factor f, for the contact points A, B, and C, were presented in Table 3. The differences between theoretical and experimental results are about 32% and 45.8% at points A and B and 12% at point C. These differences were depended on experimental arrangement (bearing model). From the results, it is concluded that a divergence is observed (Table 3), which is indebted to the accurate calculations and to the fact that there was not used separators (retainers) between rollers, thus the rollers were not been in symmetric places, as it appears in photographs.

Table 3. The concentration factors and the correction factors at the contact points A, B, and C of the bearing

Cont. points	***P* (KN)**	K_w^{th}	K_w^{ex}	$K_w^{ex} / K_w^{th} = f$
A	22.03	14.03	20.76	1.48
B	22.03	14.03	25.92	1.85
C	44.06	28.06	31.90	1.14

8. Conclusion

In the present work, the theoretical and experimental analysis of the caustics and photoelastic method were developed for the contact problem of concentrated vertical load applied at the apex of a wedge. These methods were applied to determine the stress distribution on the horizontal plane far away from the apex of the wedge. Also, the concentration factor at the apex of the wedge theoretically was determined. The concentration factor at the contact points between rings and rollers of a bearing model was experimentally determined by the experimental method of caustics. The results of the load distribution, the concentration factor, and the correction factor of the roller bearing model were presented in Table 3. The load at the wedge apex relative to the caustic characteristics were presented in Table 1.

The experimental method of caustics, which is a powerful tool for discussing fields around a crack, is also a powerful method for the contact problems and wedges with concentrated loads. Using this experimental method, the existing wedge theory may be reviewed with measurements and taking into consideration other influential parameters such as the wedge angles.

References

[1] V. M. Aleksadrov and D. A. Pozharskii, Problems of a cut in a three-dimensional elastic wedge, J. Appl. Math. Mech. 70(3) (2006), 483-492.

[2] B. G. Badalouka and G. A. Papadopoulos, Range of applicability of the method of caustics around holes, Strain 42(4) (2006), 283-290.

[3] M. Born and E. Wolf, Principles of Optics, Pergamon, London, 1970.

[4] M. M. Frocht, Photoelasticity, John Wiley, New York, 1948.

[5] Y. C. Gao, Large strain analysis of a rubber wedge compressed by a line load at its tip, Int. J. Engg. Sci. 36(7-8) (1998), 831-842.

[6] J. F. Kalthoff, Shadow Optical Method of Caustics, Handbook on Experimental Mechanics, A. S. Kobayashi (ed.), Prentice-Hall, Chapt. 9 (1987), 430-500.

[7] G. A. Papadopoulos (editor), Fracture Mechanics, The Experimental Method of Caustics and the Det.-Criterion of Fracture, Springer-Verlag, London, 1993.

[8] G. A. Papadopoulos, Experimental estimation of the load distribution in bearing by the method of caustics, Exp. Mech. 44(4) (2004), 440-443.

[9] G. A. Papadopoulos, Experimental study of the load distribution in bearing by the method of caustics and the photoelasticity method, J. Strain Analysis 40(4) (2005), 357-365.

[10] A. R. Shahani, Some problems in the antiplane shear deformation of bimaterial wedges, Int. J. Solids Struct. 42(11-12) (2005), 3093-3113.

[11] V. A. Spitas, G. K. Sfantos, Th. Costopoulos, C. A. Spitas and G. A. Papadopoulos, Numerical and Experimental Analysis of Load Sharing in Multiple Gear Tooth Contact, 7th National Congress on Mechanics, June 24-26, Chania, Greece, Proceedings 1 (2004), 232-237.

[12] V. A. Spitas, G. A. Papadopoulos, C. A. Spitas and Th. Costopoulos, Experimental Investigation of Load Sharing in Multiple Gear Tooth Contact Using the Stress-Optical Method of Caustics, Strain, 2009. Doi: 10.1111/j.1475-1305.2008.00558.x

[13] P. S. Theocaris, Local yielding around a crack tip in Plexiglas, J. Appl. Mech. 37 (1970), 409-415.

[14] P. S. Theocaris, Stress-singularities due to uniformly distribution loads along straight boundaries, Int. J. Solids Struct. 9 (1973), 655-670.

[15] P. S. Theocaris, Stress-singularities at concentrated loads, Exp. Mech. 13 (1973), 511-518.

[16] S. P. Timoshenko and J. N. Goodier (editors), Theory of Elasticity, McGraw Hill, New York, 1970.

■